Committee 4
Treatment of Non-linear Systems in
Physics and Economics

DRAFT--Sept. 12, 1997
For Conference Distribution Only

DISCOVERY OF NEW STRUCTURES - GIANT ANTICYCLONES - IN DISKS OF SPIRAL GALAXIES

by

Alexei M. Fridman
Head
Department of Physics of Stellar and Planetary Systems
Institute of Astronomy
Russian Academy of Sciences
Moscow, RUSSIA

The Twenty-first International Conference on the Unity of the Sciences
Washington, D.C. November 24-30, 1997

Discovery of new structures — giant anticyclones — in disks of spiral galaxies.

A.M.Fridman, O.V.Khoruzhii, V.V.Lyakhovich, V.S.Avedisova
Institute of Astronomy of the Russian Academy of Science, 48, Pyatnitskaya St., Moscow, 109017, Russia
O.K.Sil'chenko, A.V.Zasov, A.S.Rastorguev
Sternberg Astronomical Institute, Moscow State University, University prospect, 18, Moscow, 119899, Russia
V.L.Afanasiev, S.N. Dodonov
Special Astrophysical Observatory of the Russian Academy of Sciences, Zelenchukskaya, Stavropol'skij Krai, 377140, Russia
J. Boulesteix
Observatoire de Marseille, Place le Verrier, F-13248, Marseille, Cedex 04, France

Abstract

Overlined are general ideas as well as experimental and theoretical efforts leading to prediction of the existence of new structures in disks of spiral galaxies — giant anticyclones. Recent achievements resulted in discovery of these structures in real galaxies are described in detail. A crucial point is a new method for restoration of the full vector velocity field of the galaxy from the map of the line-of-sight velocity. Its efficiency is shown by the example of the restoration of velocity field of the galaxy NGC 157. Results for this and some other spiral galaxies are presented which demonstrate the universal existence of giant anticyclones in galactic disks.

1 Introduction

Purpose of the work is to prove, that observed over the century since their description in 1845 by Lord Rosse, the galactic spiral arms are always accompanied by giant vortices as different parts of an uniform spiral-vortex structure. While spiral arms are visible in galactic disks as the regions of increased surface density, the giant vortices are the features of velocity field of the galaxy, and, as a rule are located between spiral arms in the regions of reduced surface density. Being rather attractive and dynamical in their forms, spiral arms decorate a cover of the numerous books on astronomy. But these forms a little can tell to the observer about the dynamic process which produces the structure. In contrast, the giant vortices are carriers of a basic dynamic information about a galactic

disk. First, the centers of vortices are located near a co-rotation circle, where azimuth rotation velocities of a spiral pattern and disk coincide. The pattern speed of the spiral-vortex structure being the crucial parameter for different theories of the spiral structure is a subject of long-standing controversies. Second, disposition of centers of vortices relative to spiral arms in combination with the form of rotation curve of the disk in a neighborhood of co-rotation indicate would the mechanism of the structure generation gravitational or hydrodynamic. It should be noted that making such inference by the form of spiral arms is impossible.

The statement about existence of new structures in spiral galaxies, giant anticyclones, is based on a hypothesis of the Lindblad (1938, 1941, 1042, 1947, 1948) about a wave nature of galactic spirals. This hypothesis was laying in a base of a set of the developed theories of spiral structure (Lin and Shu 1964, 1966; Fridman 1978; Lin and Lau 1979; Fridman and Polyachenko 1984; Bertin et al 1989; Fridman 1990). Numerous observational confirmations of this hypothesis can be found in the quoted above literature and references there. The detection of vortex structures is one more confirmation of a wave nature of galactic spirals.

2 Qualitative picture of formation of anticyclones

Now let us try to understand at a qualitative level, why the velocity field of any density wave should inevitably contain the giant anticyclones.

In a laboratory an angular velocity of rotation of a disk $\Omega_L(r)$ monotonically decreases with radius function (Fig. 1a). The spiral structure, being wave density, rotates with a constant angular velocity $\Omega_{ph} = \text{const}$. A cross point of the graphs of two functions $\Omega_L(r)$ and $\Omega_{ph} = \text{const}$ corresponds to a co-rotation radius r_c. If now the observer from a laboratory frame will pass on a rotating disk, and move in radial direction, at the radius $r = r_c$ he finds the spiral arm remaining fixed (stationary). The parts of a disk interior concerning a circle $r = r_c$ will rotate faster than the spiral arm (sign " + " on Fig. 1b), and the exterior areas of a disk will lag behind.

So, in an absence of instability in a neighborhood of a co-rotation circle spiral arms are motionless, that is magnitudes of surface density and the velocities do not depend on time:

$$\sigma(r,\varphi) = \sigma_0(r) + \sigma_1(r,\varphi) = \sigma_0(r) + \tilde{\sigma}(r)\cos(2\varphi - F_\sigma)\,, \tag{1}$$

$$v_r(r,\varphi) = v_{1r}(r,\varphi) = \tilde{v}_r(r)\cos(2\varphi - F_r)\,, \tag{2}$$

$$v_\varphi(r,\varphi) = v_{0\varphi}(r) + v_{1\varphi}(r,\varphi) = v_{0\varphi} + \tilde{v}_\varphi(r)\cos(2\varphi - F_\varphi)\,. \tag{3}$$

Here the indexes "0" and "1" designate, respectively, stationary and perturbed parameters of the disk, amplitudes of perturbations are marked by "tilde", F are phases. For example

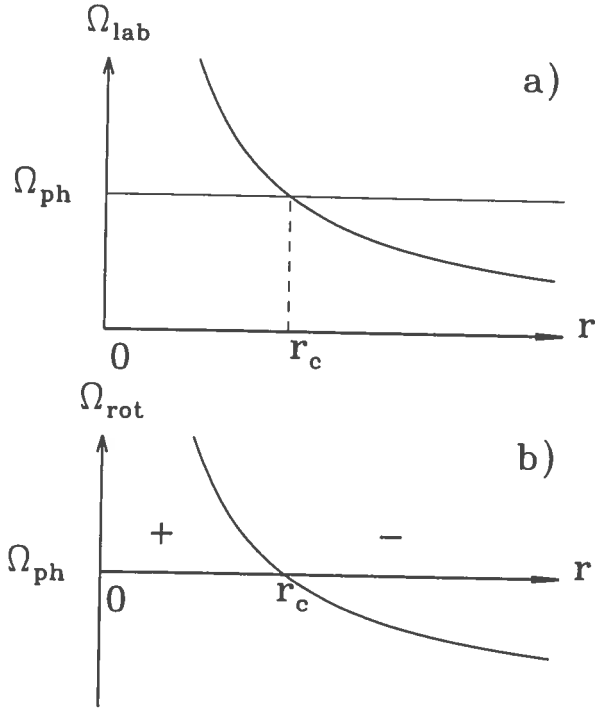

Figure 1: Radial dependence of the angular velocity of rotation of the disk: a) in the laboratory reference frame (Ω_{lab}); b) in the frame rotating with phase velocity (Ω_{ph}) of spiral structure. In the latter case the disk is stationary on the radius of corotation r_c. Signs "+" and "-"in Fig. 1b shows that the direction of the disk rotation changes the sign on the corotation radius.

we consider a two-armed spiral that is implied by the value 2φ standing in the total phases of perturbed functions.

According to (1) the perturbed surface density $\sigma_1(r, \varphi)$ for given r changes its sign with azimuth four times (double number of spiral arms). Respectively, both velocity components $v_{1r}(r, \varphi)$ and $v_{1\varphi}(r, \varphi)$ change sign with azimuth four times also. As a result in the vicinity of a corotation circle we obtain two anticyclonic vortices (Fig. 2).

Above drawn qualitative picture of the anticyclone formation in galactic disks is based on the wave nature of spiral arms only. It is universal and independent of either the disk composition (gaseous or stellar) or the nature of the mechanism generating the spiral (gravitational or hydrodynamical)[1]

[1]The location of anticyclones relative to the spiral arms depend on the details of the main parameters of the system in the corotation region. Details see in Lyakhovich et al. 1996.

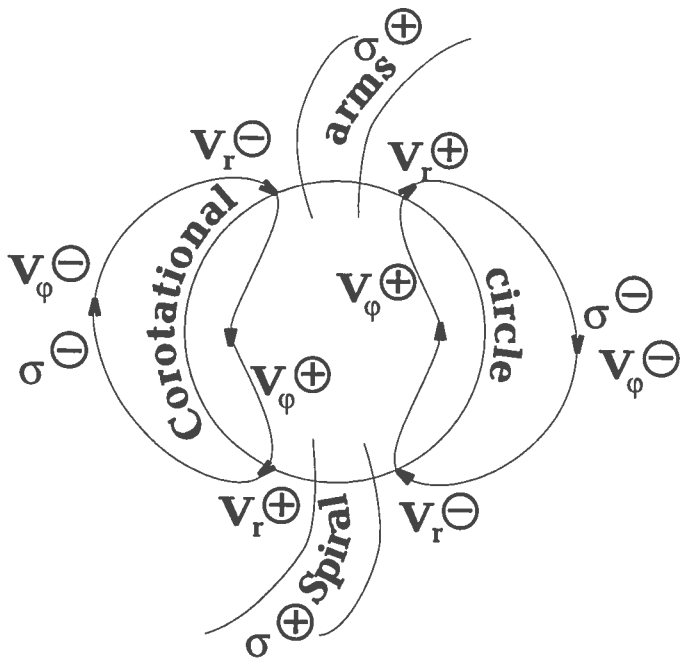

Figure 2: On the formation of two anticyclons in a neighborhood of the corotational circle in the galactic disk with two-armed spiral. In spiral arms the perturbation of the surface density of the disk is positive (sign "+"), while between arms it is negative (sign "-"). Thus sign of the density perturbation changes four times as one goes the total revolution along the azimuth. The radial velocity behaves in the same manner, that is changes its sign four times also. In the reference frame rotating with spiral structure signs of the azimuthal velocity are different on the opposite sides from the corotation circle (see Fig. 1b). As a result the velocity field near a corotation radius has a form of two anticyclones.

3 Proof of the equivalency of the linearized dynamical equations of the Galactic gaseous disk and rotating shallow water

It was shown by Fridman (1990) that the perturbed gravitational potential $\tilde{\Psi}$ in the Galactic gaseous disk is determined only by the perturbed surface density of gaseous disk $\tilde{\sigma}_g$ as in the Galaxy the perturbed surface density of stellar disk $\tilde{\sigma}_*$ is negligible in comparison with $\tilde{\sigma}_g$. Thus

$$\tilde{\Psi} = -\frac{2\pi G\tilde{\sigma}_g}{R_g|k|}, \tag{4}$$

where k is the wavenumber of the perturbation and $R_g > 1$ is a "reduction factor" allowing for the thickness.

Then the system of linearized dynamical equations for the gaseous disk in the Galaxy can be written in the following form:

$$\frac{\partial v_{1r}}{\partial t} + \Omega_0 \frac{\partial v_{1r}}{\partial \varphi} - 2\Omega_0 v_{1\varphi} = -\frac{\partial}{\partial r}(c_{g,0}^2 \eta_1), \tag{5}$$

$$\frac{\partial v_{1r}}{\partial t} + \Omega_0 \frac{\partial v_{1\varphi}}{\partial \varphi} - \frac{\kappa^2}{2\Omega_0} v_{1r} = -\frac{1}{r}\frac{\partial}{\partial \varphi}(c_{g,0}^2 \eta_1), \tag{6}$$

$$\frac{\partial \eta_1}{\partial t} + \Omega_0 \frac{\partial \eta_1}{\partial \varphi} + \frac{\partial v_{1r}}{\partial r} + (1 + r(\ln \sigma_0)') \frac{v_{1r}}{r} + \frac{1}{r}\frac{\partial v_{1r}}{\partial \varphi} = 0, \tag{7}$$

where

$$c_{g,0}^2 \equiv c_{s,0}^2 - \frac{2\pi G \sigma_0}{|k| R_g}, \quad c_{s,0}^2 \equiv \frac{dP_0}{d\sigma_0}, \quad \eta_1 \equiv \frac{\sigma_1}{\sigma_0}. \tag{8}$$

As before, we denote stationary and perturbed values by subscripts "0" and "1", respectively. In writing these equations, we have used that according to a linearised equation of state $P_1 = c_{s,0}^2 \sigma_0 \eta_1$.

If we make in system (2)–(4) the substitutions $c_{g,0}^2 = c_{w,0}^2 \equiv gH_0$, and $\eta_1 = H_1/H_0$, where g is the gravitational acceleration on the surface of the Earth, H is a shallow water depth, we obtain the system of linearized equations for rotating shallow water (Pedlosky 1982).

4 Discovery of anticyclonic vortices between spiral density waves on rotating shallow water

The previous item gives the basis to use the rotating shallow water for modeling dynamical processes in the Galactic gaseous disk. The setups "Spiral" with shallow water, rotation curve of which is similar to that of the Galactic disk, were built at the Russian Research Center "Kurchatov Institute". (Morozov et al. 1984, 1985; Fridman et al. 1985). In Fig. 3 we can see three interarm anticyclones (Nezlin et al.,1986).

Discovery of anticyclones between spiral arms in the modelling experiments with rotating shallow water stimulated a search for similar structures in spiral galaxies.

5 A vortex structure in the gaseous disk of the galaxy Mrk 1040

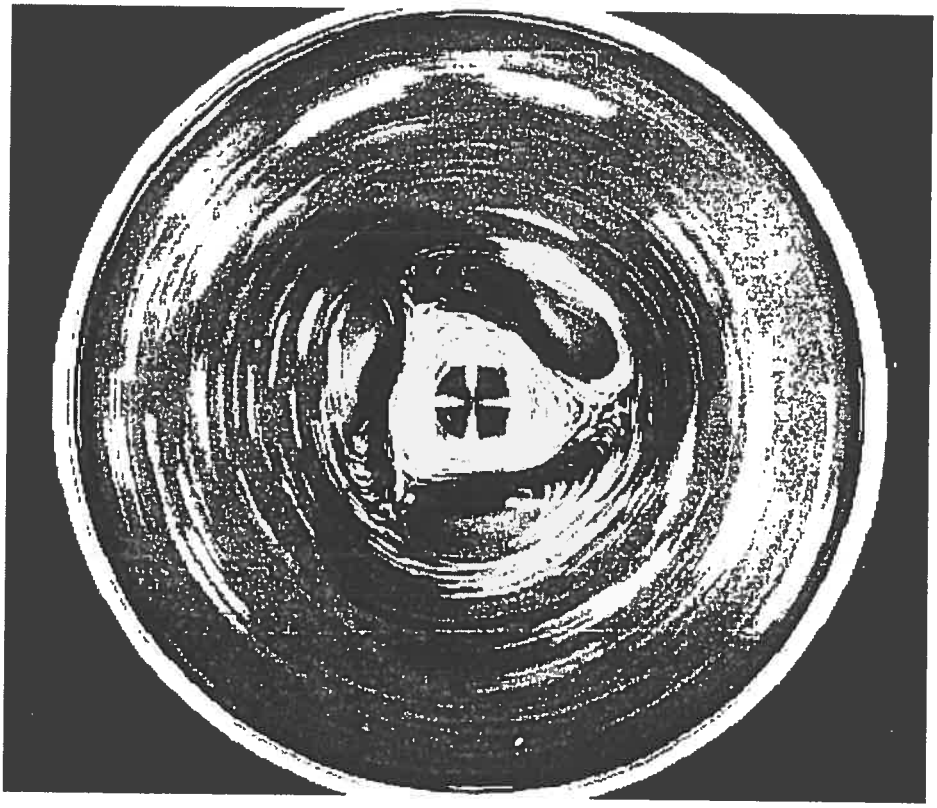

Figure 3: Spiral-vortex structure excited in shallow water; the camera rotates with the pattern.

In Fig. 4 we can see the field of residual velocities in the gaseous disk of Mrk 1040 (Afanasiev, Fridman 1993), which is obtained by subtracting an azimuthally symmetric component of the rotation curve from the line-of-sight velocity field. The structure of residual velocities shows the presence of two symmetrically located anticyclonic vortices, the external appearance of which coincides fully with the picture of anticyclonic vortices in the laboratory experiments on "shallow" water (Nezlin et al., 1986). The observed size of the anticyclones is about 4 kpc, and the velocity amplitude (in projection) is about 25 km/s.

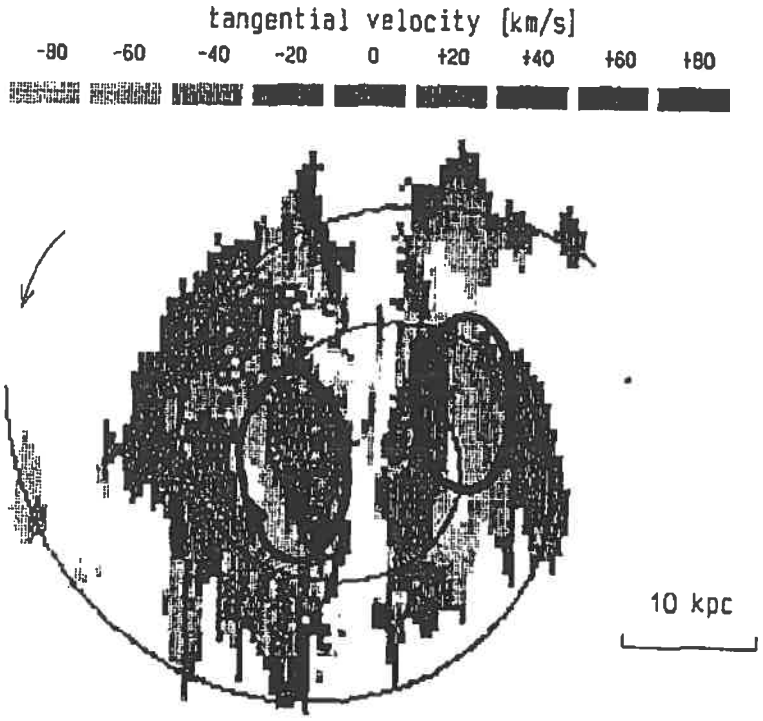

Figure 4: The field of residual velocities in the gaseous disk of Mrk 1040, in the plane of the galaxy. The near side of the galaxy is below, and an arrow shows the direction of rotation. The regions of vortices are marked by closed curves.

6 Are there giant anticyclones near the solar circle?

The velocity depression as large as 20-30 km/s on the rotation curve of the Galaxy in the solar vicinity served as a cause to put forward an assumption on the presence of an anticyclone in this region (Fridman 1994). The reconstruction of 2D vector velocity field based on the line-of sight velocity data for 312 star-forming regions (H II regions, Avedisova 1997, see Fig. 5) has shown that velocities of gas clouds inside 3-4 kpc from the Sun can be explained by an anticyclone (Fig. 6) with a center near the solar orbit between the spiral arms (Fridman et al. 1996).

We tried to check if young stellar populations would retrace the anticyclonic struc-

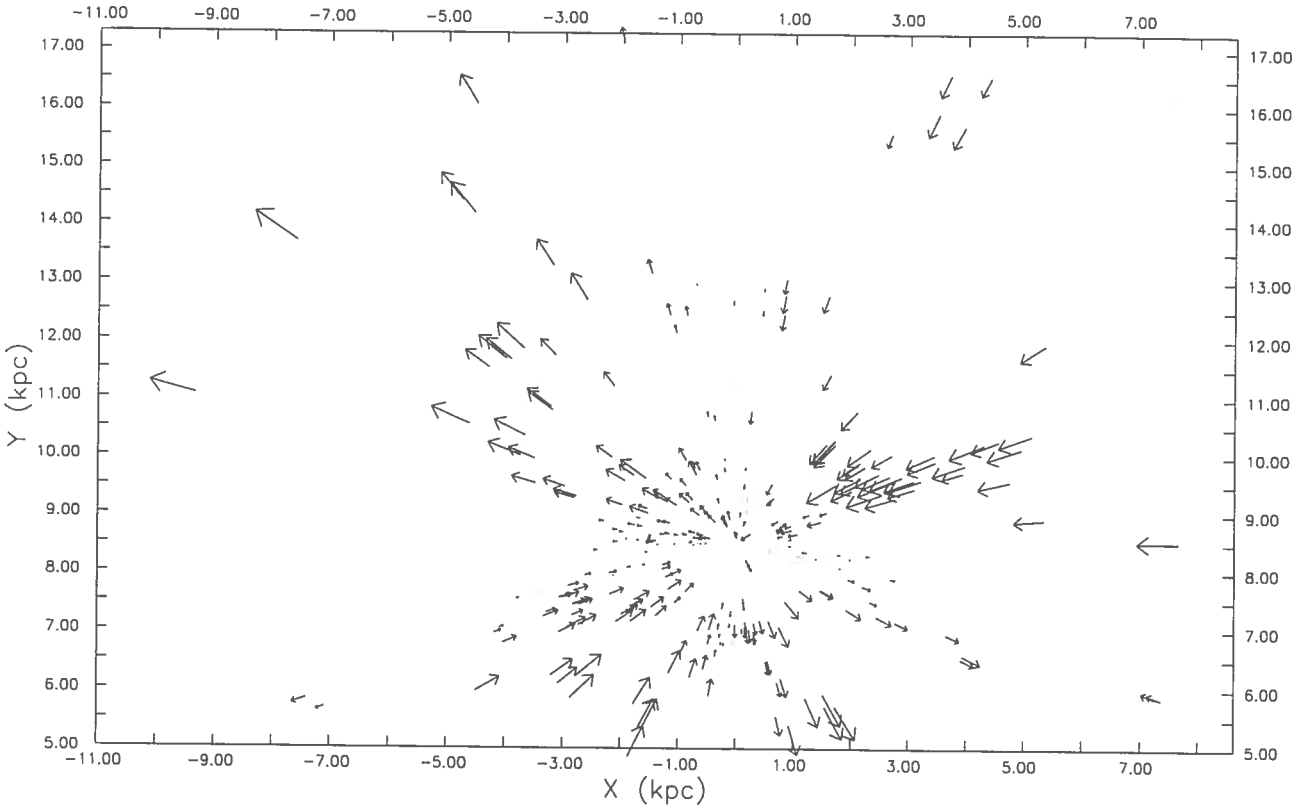

Figure 5: Line-of-sight radial velocity field of the sample 316 molecular clouds. The Sun at (0,8.5)

ture of gas in the solar vicinity.

Our sample (Rastorguev, 1997) includes approximately: 256 classical cepheids, pulsating in fundamental mode; 106 young open clusters with $t \leq 10^8$y, 99 K-M supergiants taken from Wing's (1970) list and 316 molecular clouds (Avedisova 1997).

The restoration of 2D vector velocity field based on the line-of-sight velocity data for young stellar objects has shown that they retrace the same path of gaseous clouds, forming anticyclone (Fig. 7).

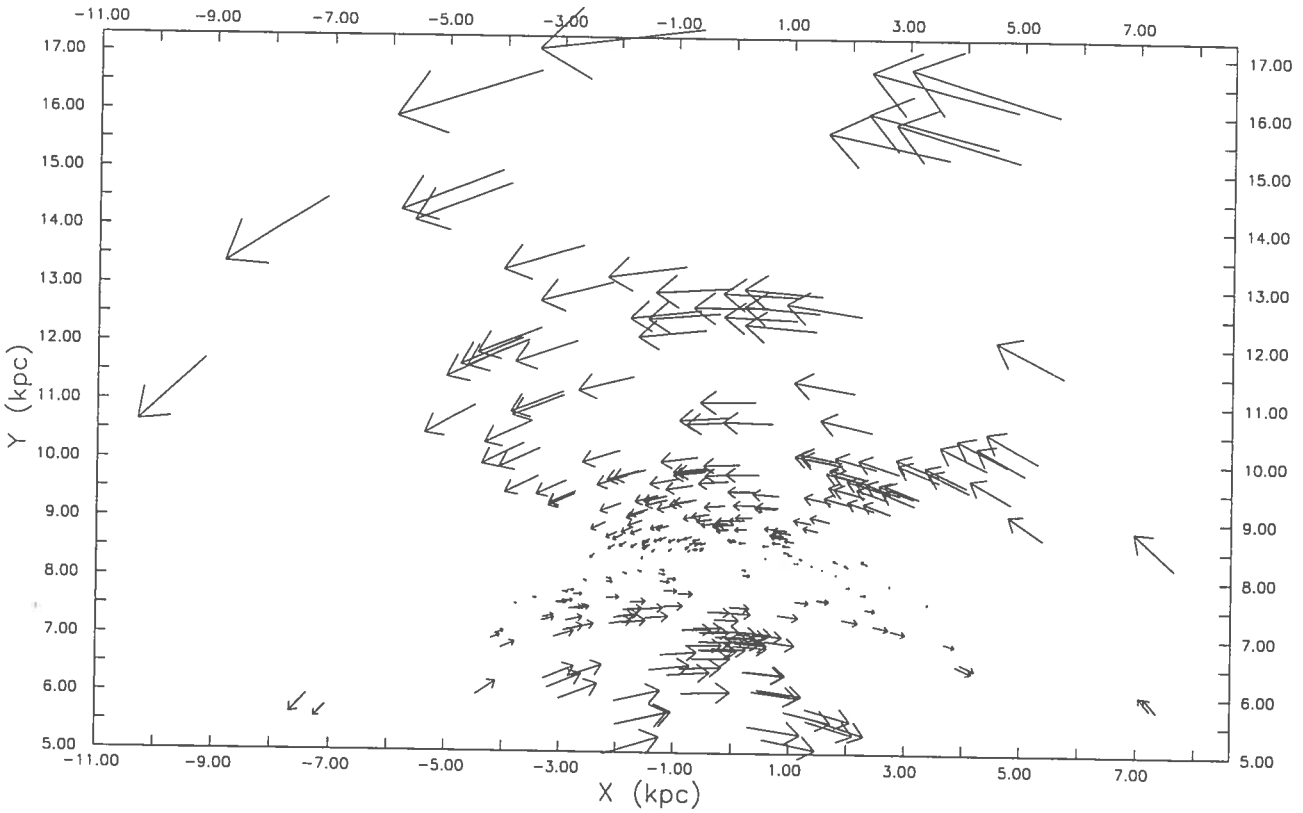

Figure 6: The full velocity field of the clouds has the form of an anticyclone with the center in solar vicinity.

7 A method for restoration of the full vector velocity field of the galaxy from the map of the line-of-sight velocity

In the work Lyakhovich et al. 1997 propose the method to restore the full vector velocity field of the galaxy from the map of the line-of-sight velocity. It is based on the following general points.

1. Appearance of azimuthal variations of density are intrinsically related with existence of peculiar velocities (azimuthally varied). As a result we expect to observe dynamically significant velocity residuals everywhere we observe noticeable density variations.

2. Errors in determination of main parameters of the galactic disk such as the center position, the inclination and the position angle of the line of nodes result in artificial addi-

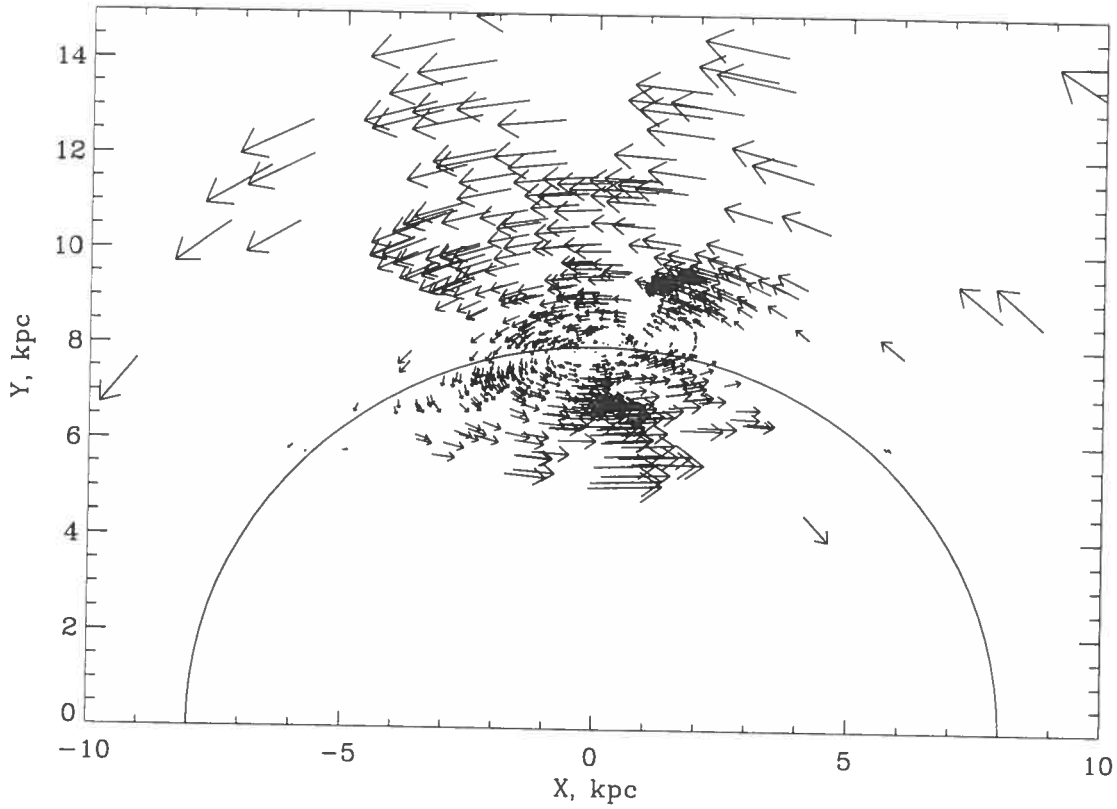

Figure 7: Line-of-sight radial velocity field of the sample of 461 stellar objects and 316 molecular clouds. The Sun is at (0,8).

tives to the observed pattern of velocity residuals. Vice versa, the presence of noncircular velocities can be mistakenly treated (in model of pure circular motions) as the radial variation of the galactic disk parameters (Lyakhovich et. al, 1997). For example neglecting azimuthal velocity variations with amplitude about 20 km/s under circular velocity about 200 km/s can result in errors in determination of inclination and position angle about 5 - 10 degrees.

3. The existence of obvious grand design in a galaxy is a consequence of one mode domination which should manifest itself by the domination of the relevant Fourier harmonic in density and velocity fields.

Due to effect of projection the m-th harmonic of galactic velocity field produces three harmonics in line-of-sight velocity field. More particularly, the m-th azimuthal and radial velocity components (in galactocentric system of reference) leads to appearance of the (m-1)-th and (m+1)-th harmonics in line-of-sight velocity while the m-th vertical velocity component (velocity component along rotation axis) causes the m-th line-of-sight

velocity harmonic.

Consequently, if we observe the domination of m-th harmonic in density field of the galaxy and (m-1)-th, m-th and (m+1)-th harmonics in line-of-sight velocity residuals (that is after subtraction of the rotation velocity) we should conclude the presence of the m-arm density wave in the galaxy and can use the observed distributions to obtain parameters of the wave.

4. The rotation velocity contributes in the cosine component of the first harmonic of line-of-sight velocity (we assume that the position of line of nodes corresponds to $\theta = 0, \pi$). As a result, if $m > 2$ the rotation curve of the galaxy and all components of the velocity residuals can be determined independently. Under this condition from observations we obtain six parameters — amplitudes and phases of (m-1)-th, m-th and (m+1)-th harmonics of line-of-sight velocity field, which allow to calculate six unknowns — amplitudes and phases of three components of m-th harmonic of residual velocity vector.

For two–arms spirals the situation is worse as the influences of rotation velocity and motions in a density wave on the line-of-sight velocity interfere with each other. In this case six observed parameters — amplitudes and phases of first, second and third harmonics of line-of-sight velocity field, are related to seven unknowns and to deduce them one needs an additional condition.

Generally speaking, the latter being theoretically deduced will be inevitably a model–dependent. Thus the problem arises to choose the condition which is as universal as possible. From this point of view choose of the particular spiral form (for example logarithmic) or WKB approximation are obviously unappropriate.

In our method we propose to use some relations between velocity residual characteristics which follows only from the wave nature of the disk perturbations. It means that different characteristics of the perturbations correspond to one self-consistent structure with some pattern speed and they are related by the hydrodynamic equations for the gaseous galactic disk. Furthermore, relations between phases of perturbations are the most suitable in our opinion. First, it can be expected that these relations do not depend on the coordinate across the disk and consequently they are not affected by the inevitable averaging of observational data trough the disk width along the line of sight. Second, as was shown by Fridman, Petviashvili and Abramyan phase position of the maximum of the perturbed density changes only slightly as the wave becomes nonlinear. Thus one can expect that the relations between phases obtained from the linearized equations will be true for any wave. The last fact can be supported by the note that despite the highly nonlinear character of the density perturbations the velocity perturbations are in any case much smaller than the rotational velocity and in this respect are quasi-linear. One can expect that the quasi-linear approximation will be the more accurate, the more dominative is the main harmonics in observations.

5. In absence of any undeniable theory of the galactic spirals any apriori relation

between different perturbation components can become occasionally wrong is some parts of the disk. To avoid this problem different (independent to some degree) conditions should be tried with use of various observational information. In our method we explore two approaches. In first we use the relation between phases of azimuthal and radial velocity components. In another the relation between phases of density perturbation and radial velocity is used. In the last case the additional information includes field of gas density of the galactic disk. The final model of velocity field of the galaxy is build by comparison of results obtained by two ways. In doing so we try to reach the smoothness of different characteristics especially of the rotation curve. The later allows to obtain a reasonable mass distribution in the galaxy without problem. It should be noted that the condition of meaningful smoothness itself in addition to observed line-of-sight velocity field rather strongly restricts the possible variety of models of velocity in the galactic disk.

8 Main equations

In this section we give a brief description of main relations used in restoration of the velocity field of a galaxy. Details can be found in Lyakhovich et al. 1997.

At given position of the center of the galactic disk, the inclination i and the position angle of the line of nodes α the observed line-of-sight velocity as a function of galactocentric azimuth φ can be expanded in the Fourier series with coefficients dependent on the galactocentric radius R:

$$V^{obs} = V_s + \sum_{n=1}^{n_{max}} \left(a_n^{obs}(R) \cos n\varphi + b_n^{obs}(R) \sin n\varphi \right) \sin i \qquad (9)$$

Here V_s systematic velocity of the galaxy and n_{max} is limited by the statistical quality of the data.

If we attribute the noncircular motions to the presence of the density wave we obtain the model representation of the line-of-sight velocity:

$$V^{mod}(R, \varphi) = V_s + V_r(R, \varphi) \sin\varphi \sin i + V_\varphi(R, \varphi) \cos\varphi \sin i + V_z(R, \varphi) \cos i\,, \qquad (10)$$

with

$$V_r(R, \varphi) = \tilde{V}_r(R, \varphi)\,, \quad V_\varphi(R, \varphi) = V_{rot}(R) + \tilde{V}_\varphi(R, \varphi)\,, \quad V_z(R, \varphi) = \tilde{V}_z(R, \varphi)\,. \qquad (11)$$

Here V_{rot} is rotational velocity.

If the observations demonstrate the domination of a single mode with azimuthal number m thus with this accuracy we can use the following expressions for the velocity variations in the wave:

$$\tilde{V}_r(R, \varphi) = C_r(R) \cos[m\varphi - F_r(R)]\,, \qquad (12)$$

$$\tilde{V}_\varphi(R,\,\varphi) = C_\varphi(R)\,\cos[m\varphi - F_\varphi(R)]\,, \tag{13}$$

$$\tilde{V}_z(R,\,\varphi) = C_z(R)\,\cos[m\varphi - F_z(R)]\,. \tag{14}$$

Hence

$$\begin{aligned} V^{mod}(R,\,\varphi) \;=\; & V_s \;+\; \sin i\,[\,V_{rot}(R)\,\cos\varphi + \\ & +\; a_{m-1}(R)\,\cos(m-1)\varphi \;+\; b_{m-1}(R)\,\sin(m-1)\varphi \;+ \\ & +\; a_m(R)\,\cos m\varphi \;+\; b_m(R)\,\sin m\varphi \;+ \\ & +\; a_{m+1}(R)\,\cos(m+1)\varphi \;+\; b_{m+1}(R)\,\sin(m+1)\varphi\,], \end{aligned} \tag{15}$$

with Fourier coefficients related to phases and amplitudes of the velocity components as

$$a_{m-1} = \frac{C_r \sin F_r + C_\varphi \cos F_\varphi}{2}\,, \tag{16}$$

$$b_{m-1} = -\frac{C_r \cos F_r - C_\varphi \sin F_\varphi}{2}\,, \tag{17}$$

$$a_m = C_z \cos F_z \,\mathrm{ctg}\, i\,, \tag{18}$$

$$b_m = C_z \sin F_z \,\mathrm{ctg}\, i\,, \tag{19}$$

$$a_{m+1} = -\frac{C_r \sin F_r - C_\varphi \cos F_\varphi}{2}\,, \tag{20}$$

$$b_{m+1} = \frac{C_r \cos F_r + C_\varphi \sin F_\varphi}{2}\,. \tag{21}$$

If $m > 2$ the above formula allow to calculate the velocity field of the galactic disk.

For two–armed spirals the system becomes incomplete:

$$V_{rot} \;+\; \frac{C_r \sin F_r + C_\varphi \cos F_\varphi}{2} \;=\; a_1^{obs}\,, \tag{22}$$

$$-\; C_r \cos F_r \;+\; C_\varphi \sin F_\varphi \;=\; 2\,b_1^{obs}\,, \tag{23}$$

$$-\; C_r \sin F_r \;+\; C_\varphi \cos F_\varphi \;=\; 2\,a_3^{obs}\,, \tag{24}$$

$$C_r \cos F_r \;+\; C_\varphi \sin F_\varphi \;=\; 2\,b_3^{obs}\,, \tag{25}$$

For tightly wound spirals $|\partial \ln f/\partial \ln R| \gg 1$ (note that this condition is much less restrictive then the WKB approximation) outside the corotation one can derive the following relations between phases of radial and azimuthal velocity perturbations:

$$F_\varphi(R) \;=\; F_r(R) \;\mp\; \pi/2\,, \quad \text{for} \quad \kappa^2 > 0\,, \tag{26}$$

$$F_\varphi(R) \;=\; F_r(R) \;\pm\; \pi/2\,, \quad \text{for} \quad \kappa^2 < 0\,. \tag{27}$$

The upper sign correspond to the region before the corotation $R < R_c$, the lower — to the region after corotation $R > R_c$. It is seen that the relation between phases is 'switched' on corotation. As the phases are fixed up to the $\pm 2\pi$ only, the way of the 'switching' can be different. It can be shown that in each particular case the way is determined by the spirals type (leading or trailing) and the direction of the disk rotation in the pattern plane. For trailing spirals and $\kappa^2\Omega > 0$:

$$F_\varphi(R_c) \;=\; F_r(R_c) \;+\; \pi\,, \tag{28}$$

while for $\kappa^2\Omega < 0$:

$$F_\varphi(R_c) \;=\; F_r(R_c)\,. \tag{29}$$

Correspondent behavior of phase differences with R is shown in Figs. 8.

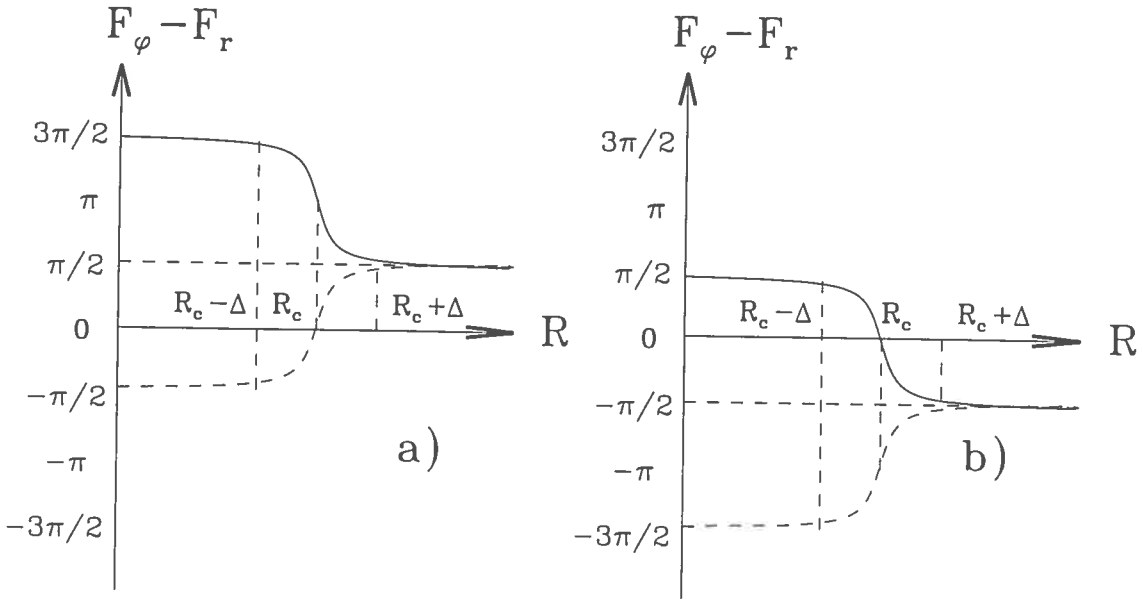

Figure 8: Schematic view of radial dependencies of the difference between phases of radial and azimuthal perturbed velocities for different orientation and parameters of the galactic disk. (a) The case $\kappa^2 > 0$, solid line — $\Omega > 0$, that is if the axe z is directed from the observer and the disk rotates clockwise; dashed line – $\Omega < 0$, disk rotates counter clockwise. (b) The same for the case $\kappa^2 < 0$.

Under condition (26) system (22) – (25) has the form:

$$V_{rot} \;=\; a_1^{obs} \;-\; \frac{1}{2}(C_r \pm C_\varphi)\,\sin F_r\,, \tag{30}$$

$$(C_r \pm C_\varphi)\cos F_r \;=\; -2\,b_1^{obs}\,, \tag{31}$$

$$(C_r \mp C_\varphi)\sin F_r \;=\; -2\,a_3^{obs}\,, \tag{32}$$

$$(C_r \mp C_\varphi)\cos F_r \;=\; 2\,b_3^{obs}\,. \tag{33}$$

This allows to restore all characteristics of the velocity field:

$$\mathrm{tg}\,F_r \;=\; -\,\mathrm{ctg}\,F_\varphi \;=\; -\,a_3^{obs}/b_3^{obs}\,, \tag{34}$$

$$\cos F_r \;=\; \mathrm{sign}\left(b_3^{obs}-b_1^{obs}\right)\sqrt{\frac{(b_3^{obs})^2}{(a_3^{obs})^2+(b_3^{obs})^2}}\,, \tag{35}$$

$$C_r \;=\; (b_3^{obs}-b_1^{obs})/\cos F_r\,, \tag{36}$$

$$C_\varphi \;=\; \mp\,(b_3^{obs}+b_1^{obs})/\cos F_r\,, \tag{37}$$

$$V_{rot} \;=\; a_1^{obs} \;-\; \frac{a_3^{obs}\,b_1^{obs}}{b_3^{obs}}\,. \tag{38}$$

As above the upper sign is for $R < R_c$ and the lower for $R > R_c$.

As the amplitudes are always positive, equations (36) and (37) are consistent only if

$$\begin{array}{ll} |b_3^{obs}(R)| - |b_1^{obs}(R)| \le 0, & \text{for} \quad R < R_c, \\ |b_3^{obs}(R)| - |b_1^{obs}(R)| \ge 0, & \text{for} \quad R > R_c. \end{array} \tag{39}$$

This condition allows to determine approximately the location of the corotation from the observations only.

As was pointed in previous section the another way to complete system (22) – (25) consists in using the information on density distribution. For this purpose we can to derive the relation between phases of the density and the radial velocity perturbations.

It can be shown that if $|\mathrm{Im}\,k| \ll |\mathrm{Re}\,k|$, where k is a wave vector of the wave, the following relations hold. Outside the corotation one has

$$\begin{array}{lll} F_r(R) \;=\; F_\sigma(R) \;+\; \pi, & \text{for} & R < R_c\,, \\ F_r(R) \;=\; F_\sigma(R), & \text{for} & R > R_c\,. \end{array} \tag{40}$$

On the corotation:

$$F_r(R_c) \;=\; F_\sigma(R_c) \;-\; \pi/2\,, \text{for} \;\; \kappa^2\Omega > 0\,, \tag{41}$$

$$F_r(R_c) \;=\; F_\sigma(R_c) \;+\; \pi/2\,, \text{for} \;\; \kappa^2\Omega < 0\,. \tag{42}$$

The approximate behavior of the phase differences with R is shown in Figs. 9.

The dependence of F_σ on R can be determined by the analysis of the second Fourier harmonic of the density field. At known $F_\sigma(R)$ from (40) and (22) – (25) we obtain:

$$C_r \;=\; \mp\,\frac{b_3^{obs}-b_1^{obs}}{\cos F_\sigma}\,, \tag{43}$$

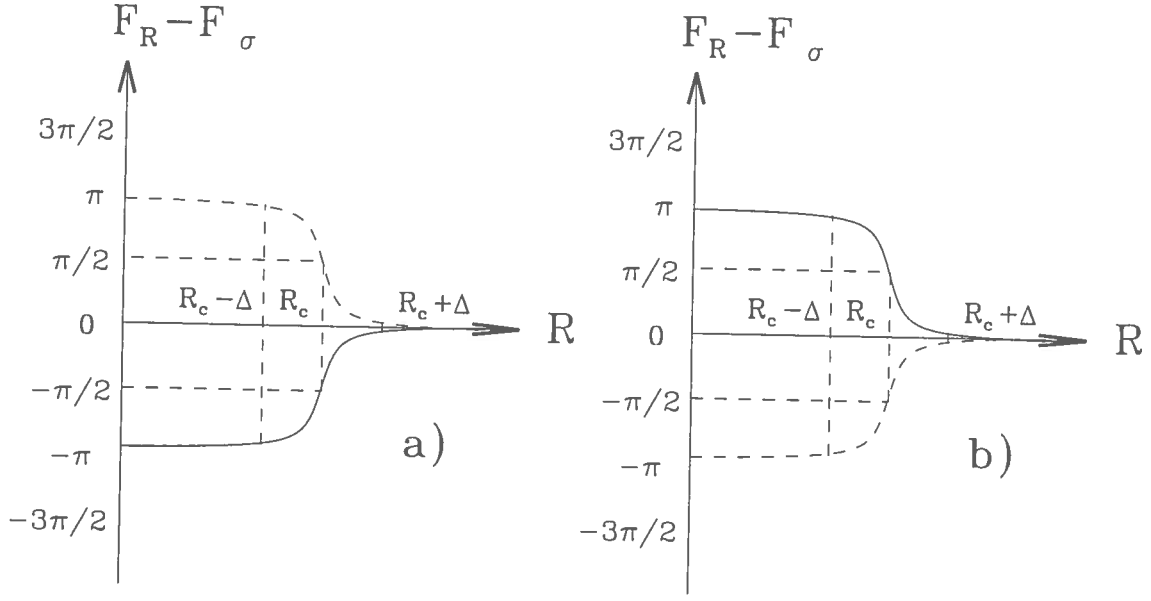

Figure 9: Schematic view of radial dependencies of the difference between phases of radial velocity and density perturbation depending on the orientation and parameters of the galactic disk. (a) The case $\kappa^2 > 0$, solid line — $\Omega > 0$, that is if the axe z is directed from the observer and the disk rotates clockwise; dashed line – $\Omega < 0$, disk rotates counter clockwise. (b) The same for the case $\kappa^2 < 0$.

$$\operatorname{ctg} F_\varphi = \frac{2a_3^{obs} + (b_3^{obs} - b_1^{obs}) \operatorname{tg} F_\sigma}{b_3^{obs} + b_1^{obs}}, \tag{44}$$

$$C_\varphi = \{(b_3^{obs} + b_1^{obs})^2 + [2a_3^{obs} + (b_3^{obs} - b_1^{obs}) \operatorname{tg} F_\sigma]^2\}^{1/2}, \tag{45}$$

$$\sin F_\varphi = (b_1^{obs} + b_3^{obs})/C_\varphi \tag{46}$$

$$V_{rot} = a_1^{obs} - a_3^{obs} - (b_3^{obs} - b_1^{obs}) \operatorname{tg} F_\sigma . \tag{47}$$

Taking into account that $C_r > 0$, from relation (43) we can deduce additional estimation of the corotation location:

$$\begin{array}{ll} (b_3^{obs}(R) - b_1^{obs}(R)) \cos F_\sigma(R) \le 0, & \text{for } R < R_c, \\ (b_3^{obs}(R) - b_1^{obs}(R)) \cos F_\sigma(R) \ge 0, & \text{for } R > R_c. \end{array} \tag{48}$$

9 Restoration of the velocity field on the example of galaxy NGC 157

Fig. 10 shows the histograms of line-of-sight velocity Fourier harmonics at different galactocentric radii of the galaxy NGC 157. It is seen that the domination of the second and third harmonics is profound for the most part of the galactic disk. Thus the method described in the previous sections can be used to restore the velocity field of this galaxy (details see in Fridman et al. 1997).

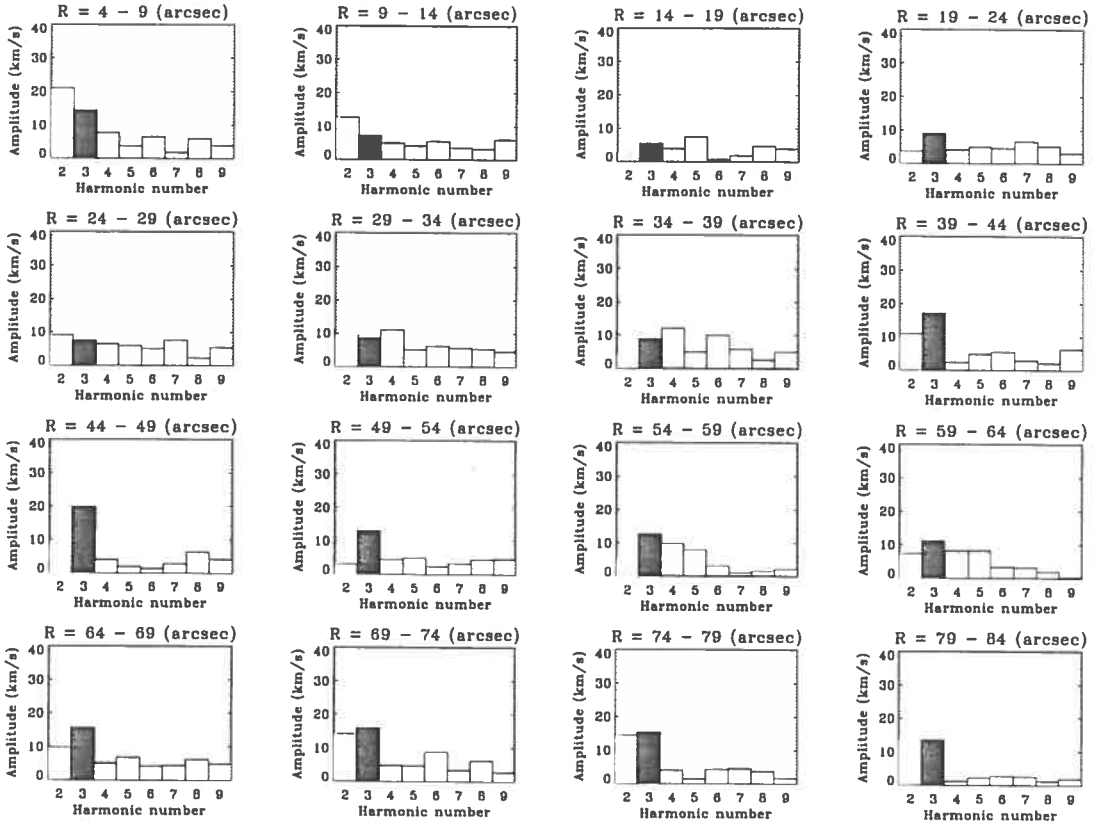

Figure 10: Histograms of line-of-sight velocity Fourier harmonics at different galactocentric radii of the galaxy NGC 157. It is seen the domination of the second and third harmonics for the most part of the galactic disk.

The radial behavior of main harmonics of the line-of-sight velocity field for NGC 157 is shown in Fig. 11.

Fig. 12 shows the behavior of $|b_3^{obs}(R)| - |b_1^{obs}(R)|$ in NGC 157. According to this data the corotation radius is about $43'' \pm 3''$.

If we use the condition (26) to complete system (22) – (25) we obtain the charac-

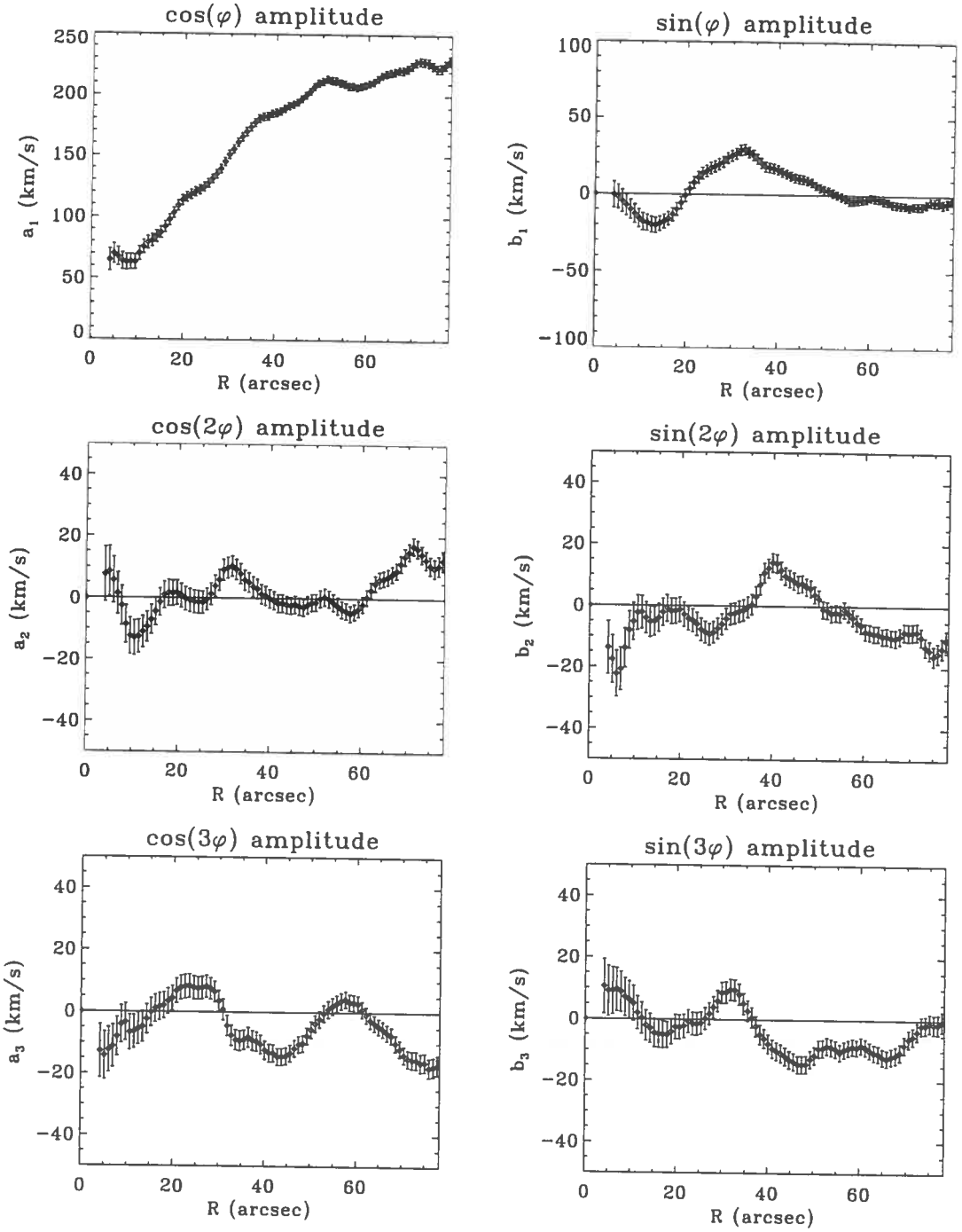

Figure 11: Radial behavior of main harmonics of the line-of-sight velocity field for NGC 157. Bars show the observational errors (3σ).

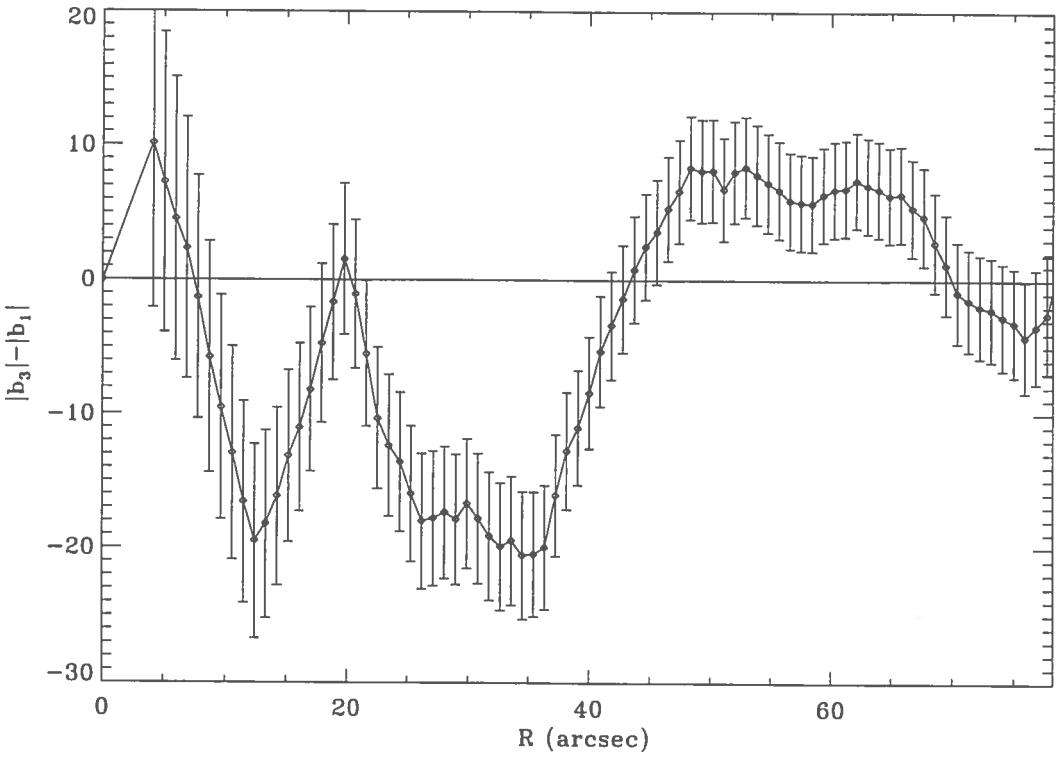

Figure 12: Behavior of $|b_3^{obs}(R)| - |b_1^{obs}(R)|$ with galactocentric radius R in NGC 157. In approximation of tightly wound spirals the difference is negative before the corotation radius and positive after the corotation. The approximation is not valid near the center and on the periphery of the galaxy. Thus according to this data the corotation radius is about $43'' \pm 3''$

teristics of velocity field represented in Fig. 13. In case of NGC 157 spirals are trailing, $\kappa^2 > 0$ and $\Omega < 0$.

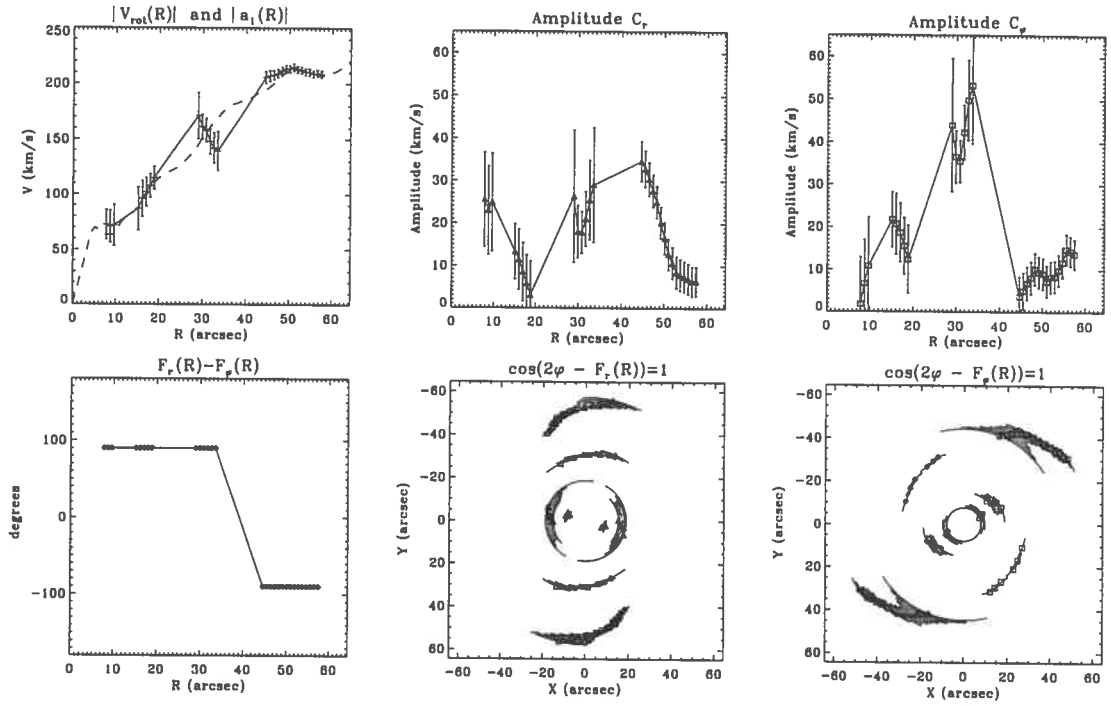

Figure 13: Characteristics of velocity field of NGC 157 obtained by the first method of the velocity field restoration, that is if we use the condition (26) to complete system (22) – (25).

Fig. 14 shows the dependence of $(b_3^{obs} - b_1^{obs}) \cos F_\sigma$ on galactocentric radius R. It is seen that the estimation on the base of condition (48) is in agreement with that from condition (39).

If we use the relation between phases of the radial velocity and density perturbations to restore velocity field, we obtain parameters shown in Fig. 15.

It should be noted that consistency of the procedures used above to complete system of equations (22) – (25) can be checked directly from the observations. Really, from equations (20) and (21) one can conclude that under conditions (26) and (40) the third harmonic of line-of-sight velocity should have a form

$$H_3 \;=\; (C_\varphi \mp C_r)\;\cos(3\varphi - F_\sigma - \pi/2)\,. \qquad (49)$$

Thus the procedures are consistent if the phase of the third harmonic of line-of-sight velocity is close to the phase of the second harmonic of density minus $\pi/2$. Fig. 16 shows the azimuthal positions of the solutions of equation $\cos(2\varphi - F_3 + \pi/2) = 1$, where F_3 is

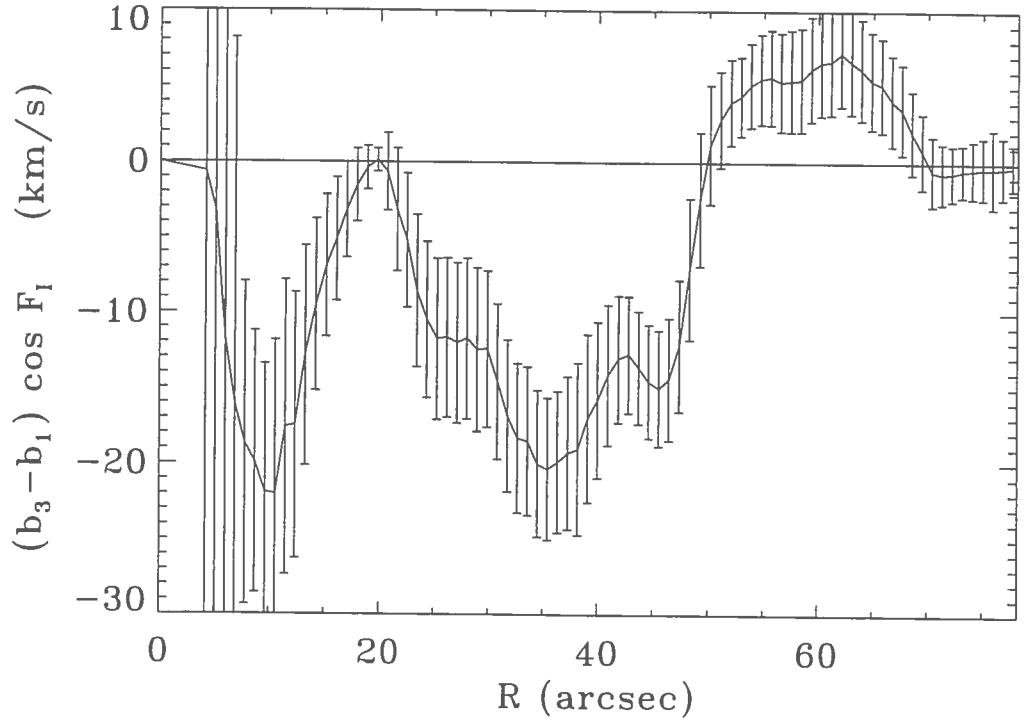

Figure 14: Behavior of $(b_3^{obs} - b_1^{obs}) \cos F_\sigma$ with galactocentric radius R in NGC 157. In WKB approximation the difference is negative before the corotation radius and positive after the corotation. The approximation is not valid near the center and on the periphery of the galaxy.

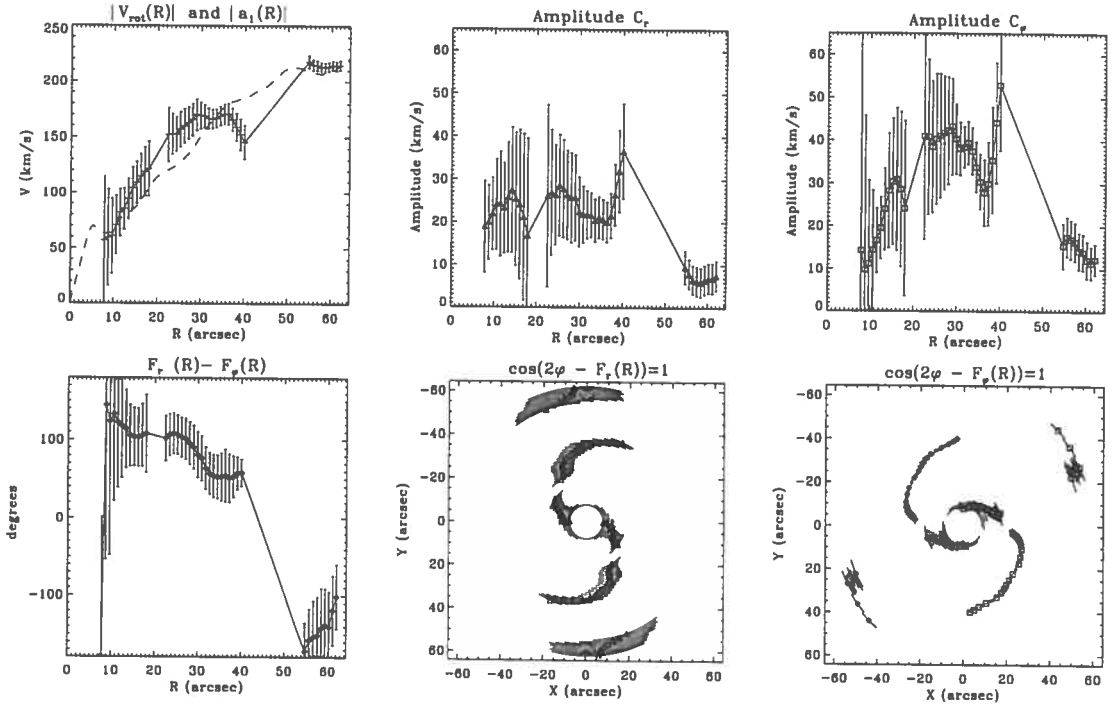

Figure 15: Characteristics of velocity field of NGC 157 obtained by the second method of the velocity field restoration, that is if we use the condition (40) to complete system (22) – (25).

a phase of the third harmonic of line-of-sight velocity, overlaid on the field of density of the gas in the galaxy. It is seen that the positions are in good corelation with the density maxima. The disagreement is relatively high only on the very periphery of the disk where the lack of the data could play a role.

At the last step the characteristics of the velocity field was varied inside the range of uncertainty limited by the two procedures described above. By this mean the smoothness of R dependencies was achieved. Final model which gives the best fit is represented in Fig. 17. Knowing the behaviour of the phase difference between radial and azimuthal velocity variations the position of the corotation can be determined more exactly by the relation (28). In described model this gives $R_c = 42''$.

The procedure described above in details for the case of NGC 157 was also performed to obtain the velocity fields of some other galaxies. Figs. 19 and 20 show some examples of the results of restoration. In all cases anticyclonic vortices are present near the corotation circle.

The velocity field in frame rotating with angular velocity $\Omega(R_c)$ is shown in Fig. 18. The presence of two anticyclones is evident.

10 Conclusions

In conclusion we reproduce main steps of the discovery of giant galactic anticyclones.

1. The existence of important dynamical feature of any spiral galaxy — giant anticyclonic vortices located near the corotation, was predicted by the successful laboratory simulation on the setups with shallow water ("Spiral"). The modeling is based on the proof of the equivalency of the dynamical equations of the Galactic gaseous disk and rotating shallow water.

2. Analysis of velocity field of Mkn 1040 demonstrates the existence of vortex structures in this galaxy.

3. An evidence for the existence of anticyclone in the solar vicinity of the Galactic disk was obtained on the base of the data for line-of sight velocities of HII regions and young stellar objects.

4. A method for restoration of the full vector velocity field of the galaxy from the map of the line-of-sight velocity was proposed.

5. Using this method the velocity field of several galaxies was restored, and universal existence of giant anticyclones in spiral galaxies was demonstrated.

The work was performed under financial support of RFFI grants N 96-02-17792 and N 96-02-19636.

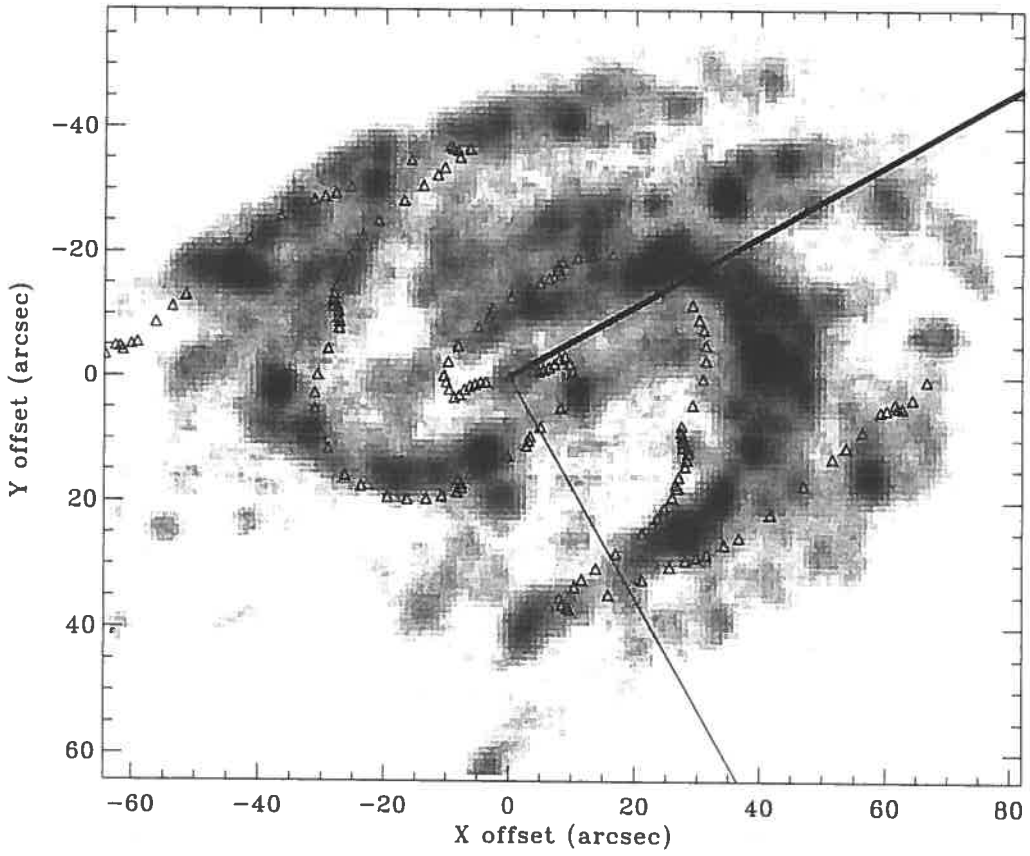

Figure 16: The correlation between the phase of the third harmonic of the line-of-sight velocity field (circles) and the density perturbation (gray scale image). The correlation proves that the observed deviations from pure rotation are caused by the spiral density wave and validity of the methods used in the paper.

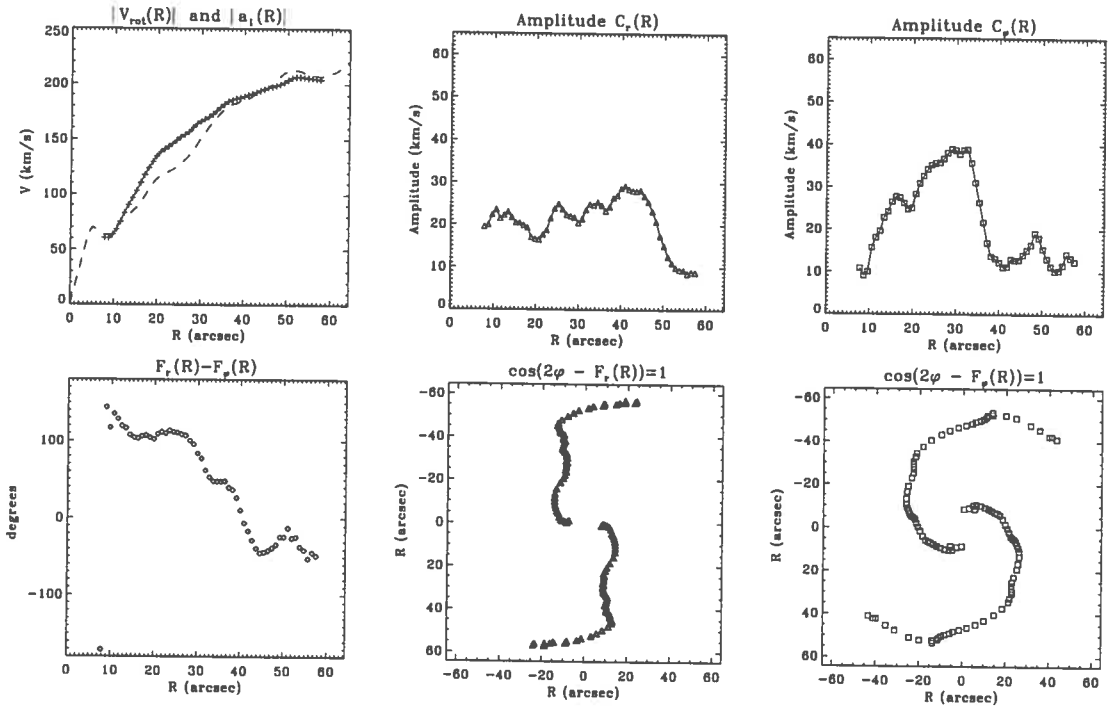

Figure 17: Characteristics of velocity field of NGC 157 obtained taking into accound both methods of the velocity field restoration. In the first figure of the set the restored rotational velocity is shown by crosses. Dashed line shows the amplitude of cosine harmonic of line-of-sight velocity wich corresponds to the rotation curve obtained in the model of pure rotation.

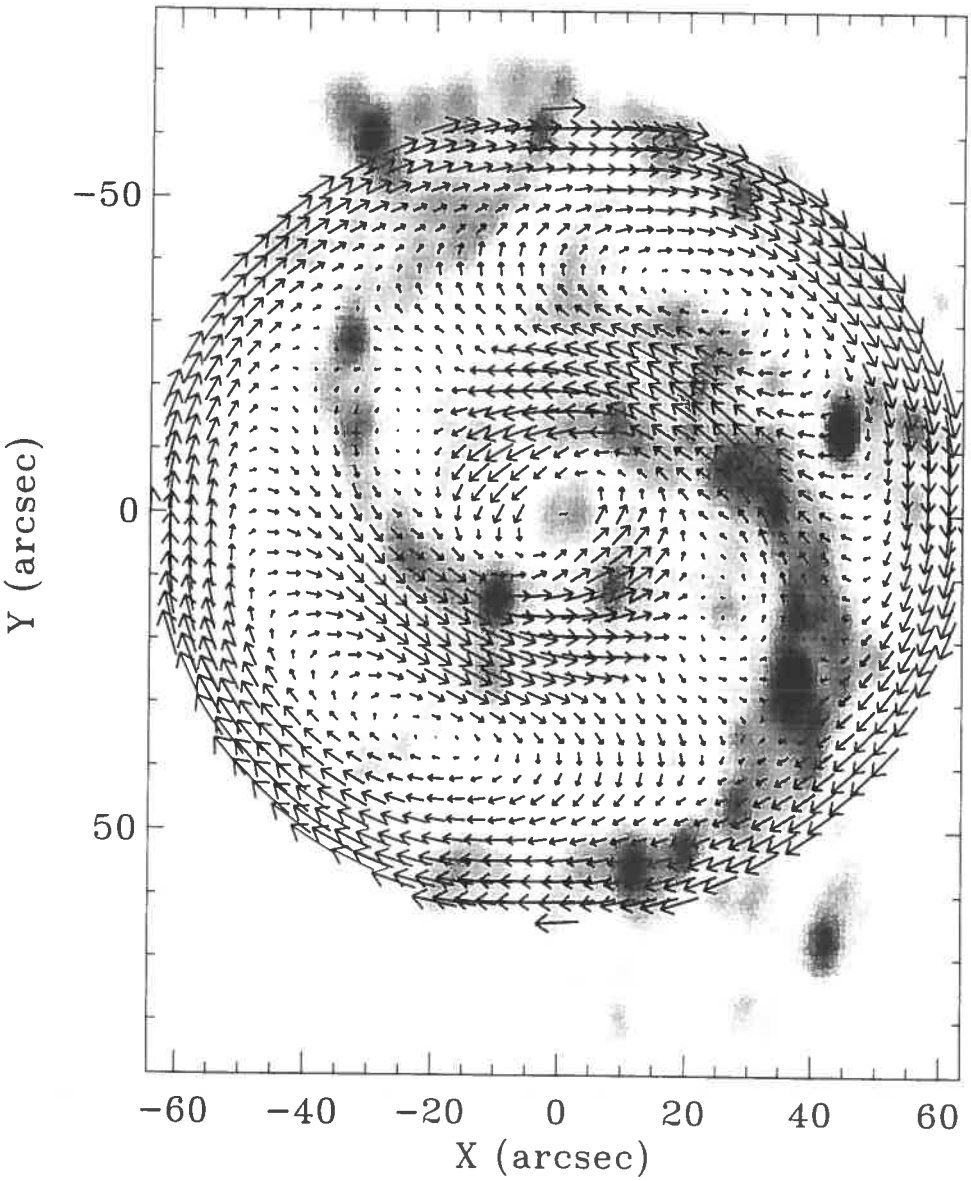

Figure 18: Restored velocity field of NGC 157 in the reference frame rotating with the partern speed of the spiral structure overlaid on the density distribution of the gas in the galaxy.

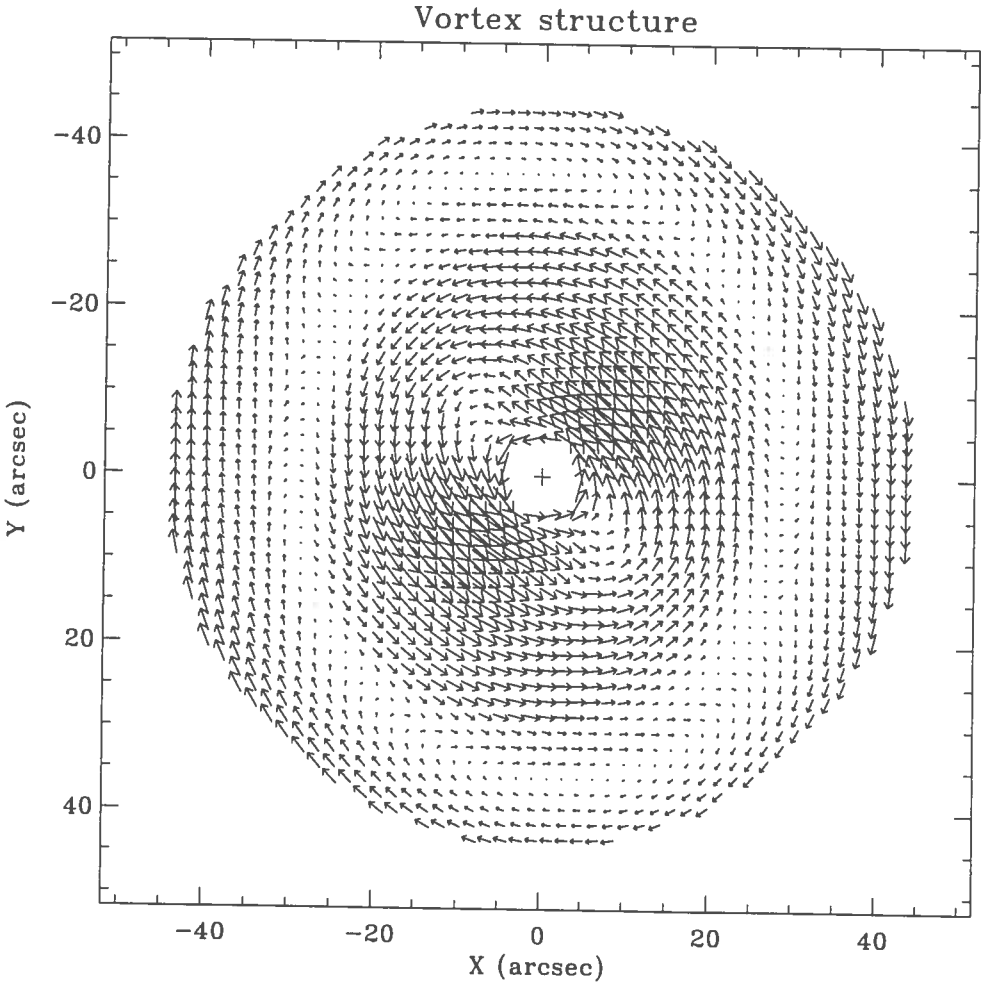

Figure 19: Restored velocity field of NGC 6181 in the reference frame rotating with the partern speed of the spiral structure.

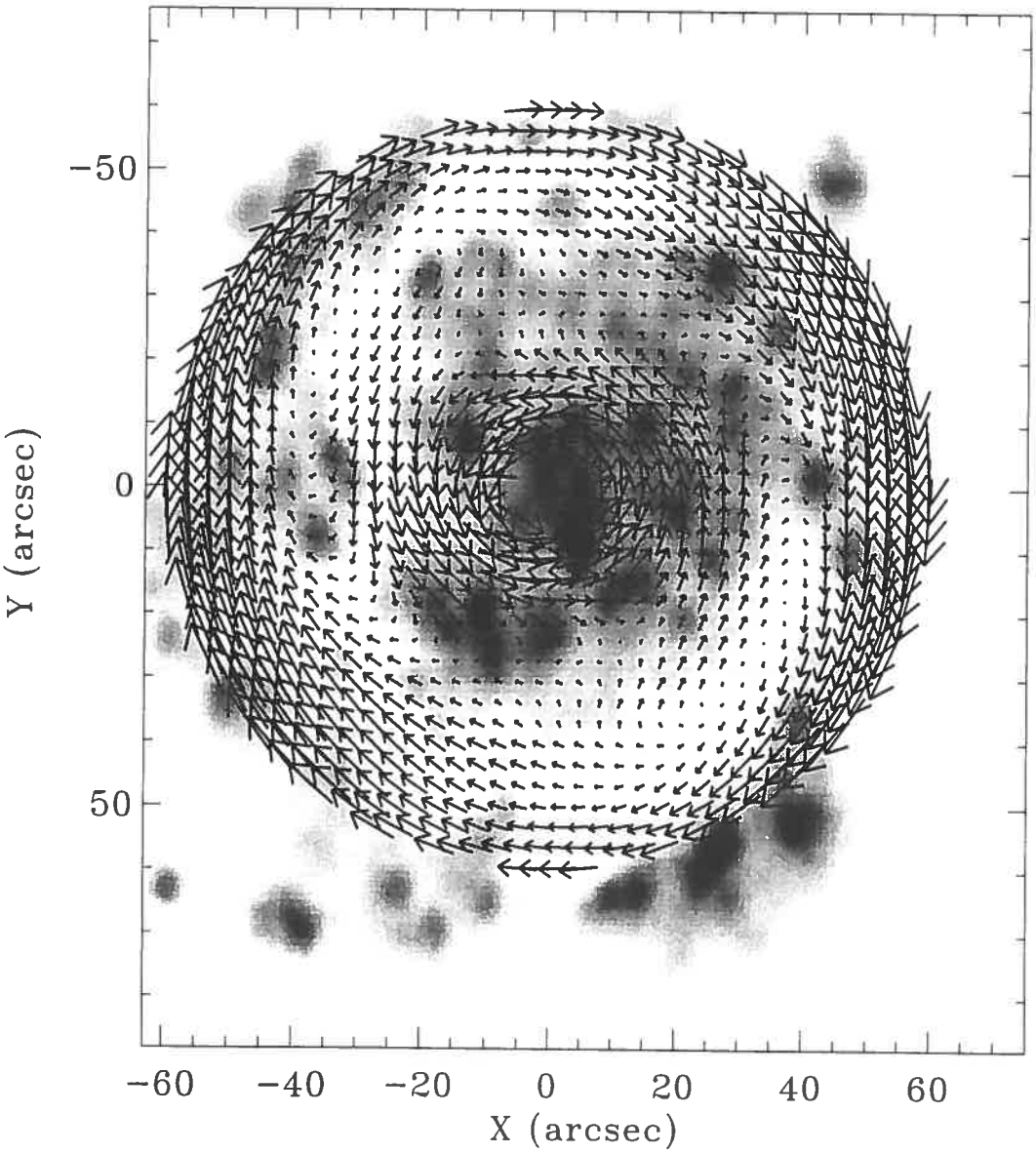

Figure 20: Restored velocity field of NGC 3893 in the reference frame rotating with the partern speed of the spiral structure overlaid on the density distribution of the gas in the galaxy.

References

1. Avedisova, V.S.// Catalogue of observational data in galactic star-forming regions, 1997, Version 2 (in preparation).

2. Lindblad B.// Zeitschr. f. Astrophys. 1938. V.15. P.124.

3. Lindblad B.// Stokholms Obs. Ann. 1941. V.13. No 10.

4. Lindblad B.//Stokholms Obs. Ann. 1942. V.14. No 1.

5. Lindblad B.//Publs. Astron. Sos. Pacif. 1947. V.59. No 305. No 351.

6. Lin C.C., Shu F.H. // Astrophys. J. 1964, V.140. P.646.

7. Lin C.C., Shu F.H. // Proc. Nat. Acad. Sci. U.S.A. 1966. V.55. P.229.

8. Lin C.C., Lau Y.Y. // Studies in Applied Mathematics. 1979. V.60. P.97.

9. Fridman A.M. // Uspekhi Fiz Nauk, 1978, V.125, P.352 & Sov. Phys. Usp. 1979, V.21, P.536.

10. Fridman, A.M., Polyachenko, V.L. // Physics of gravitating systems. N.Y. etc.: Springer–Verlag, 1984. V.1. V.2.

11. Bertin G., Lin C.C., Lowe S.A. and Thurstans R.P.// Ap.J., 1989, V.338,P.78;104.

12. Fridman A.M. // In "Dynamics of Astrophysical Disks", Edited by J.A.Sellwood, Cambridge University Press, 1990, p.185.

13. Pedlovsky J. // Geophysical Fluid Dynamics, v.1,2, Springer-Verlag, New-York, Heidelberg, Berlin, 1982.

14. Morozov, A.G., Nezlin, M.V., Snezhkin, E.N., Fridman, A.M. // JETP Lett., 1984, V.39, P.615.

15. Morozov, A.G., Nezlin, M.V., Snezhkin, E.N., Fridman, A.M. // Sov. Phys. Uspekhi, 1985, V.28, P.101.

16. Morozov, A.G., Nezlin, M.V., Snezhkin, E.N., Fridman, A.M. // Phys. Lett., 1985, A109, 228.

17. Nezlin, M.V., Polyachenko, V.L., Snezhkin, E.N., Trubnikov, A.S., Fridman, A.M. // Sov. Astron. Lett., 1986, V.12, P.213.

18. Fridman A.M., Khoruzhii O.V., Lyakhovich V.V., Avedisova V.S. // Unsolved Problems of the Milky Way / eds. Blitz L. and Teuben P. Kluwer academic publishers, Netherlands, 1996. P.597.

Fridman, A.M. // In "Physics of the Gaseous and Stellar Disks of the Galaxy", Ed. I.R.King, PASP Conference Ser., V.66., P.15.